AMSI SUMMER RESEARCH SCHOLARSHIPS 2024–25

Get a taste for Research this Summer

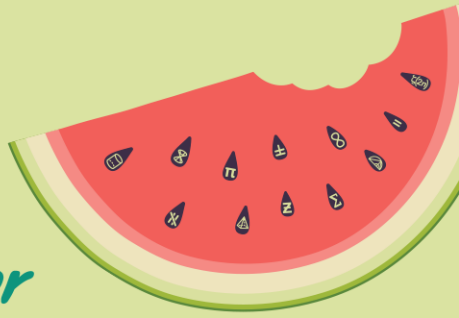

A mathematical exploration of the role of feral pigs in the transmission of Japanese encephalitis virus

Emma Naumann

Supervised by A/Prof Roslyn Hickson and Dr Justin Sexton

James Cook University and CSIRO

February 26, 2025

Abstract

Japanese encephalitis virus (JEV) is a zoonotic disease endemic in Southeast Asia and the Pacific. It is of increasing importance within Australia, as evidenced by the 2022 outbreak which killed six people, and the confirmed 2025 cases. The role of feral pigs and circumstances when endemic transmission of Japanese encephalitis virus might be maintained within Australia were investigated through a compartmental transmission model. This model included both the established pig-to-mosquito-to-pig (vector-borne) transmission cycle, and the direct pig-to-pig transmission supported by emerging evidence. A transmission model was developed to capture these transmission pathways, and analytical expressions of threshold conditions and steady states were found. The model was then parameterised using values obtained from the literature, except the pig-to-pig transmission rate which was unknown in the Australian context. We explored the impact of no, low and high scenarios for this direct transmission rate on the dynamics. Whilst an outbreak of JEV can occur without the contribution of direct pig-to-pig transmission, this model solution reduced the magnitude of peak incidence, and did not result in an endemic steady state. These results suggest that pig-to-pig transmission of JEV could be a significant contributor to the endemicity of JEV within Australia. Although we focussed on North Queensland, ongoing transmission in northern Australia has strong implications for incursions into southern regions where there are both more domestic piggeries and denser human populations, increasing risks to both agriculture and human health.

1 Introduction

Japanese encephalitis virus (JEV) is of increasing importance in Australia, as evidenced by the 2022 Australian outbreak which killed six people and infected many others (Wadman (2023)), and the confirmed 2025 cases (Goondiwindi Regional Council (2025), McGrath, Christian (2025)). JEV is a flavivirus endemic in Southeast Asia and the Pacific (Diallo et al. (2018)). Global JEV cases, whilst underreported, are estimated to be between 50,000 and 68,000 annually, with 3 billion people at risk (Diallo et al. (2018), De et al. (2016)). Approximately 20% to 30% of people who develop encephalitis die, and 30% to 60% of survivors develop long-term neurological illnesses, including tremors, paralysis, and convulsions (De et al. (2016), Khan et al. (2014)). As depicted in Figure 1, the sylvatic cycle of JEV is between wild reservoir hosts of Ardeid birds (nomadic waterbirds such as egrets and herons), with mosquitoes the primary vector, and pigs as an amplifying host (Diallo et al. (2018), De et al. (2016), Lord et al. (2015)). Humans, and several other mammals, are potential dead-end hosts (Diallo et al. (2018), De et al. (2016), Lord et al. (2015)). *Culex tritaeniorhynchus* (*Culex t.*) is the primary vector within Southeast Asia, and *Culex annulirostris* (*Culex a.*) has been identified as a possible primary vector within Australia (Diallo et al. (2018), Klein et al. (2024), Lord et al. (2015), Furlong et al. (2022)).

The transmission of JEV by mosquitoes, known as vector-borne transmission, is the primary transmission pathway (Furlong et al. (2022, 2023), Mulvey et al. (2021)). Factors such as climate can potentially result in seasonal fluctuations of mosquito populations, and hence mosquito-borne transmission: mosquito populations decline during the winter in temperate regions such as in China, Japan, and southern Australia, and during the dry season in tropical climates (Diallo et al. (2018)). Despite this, JEV transmission persists year-round within

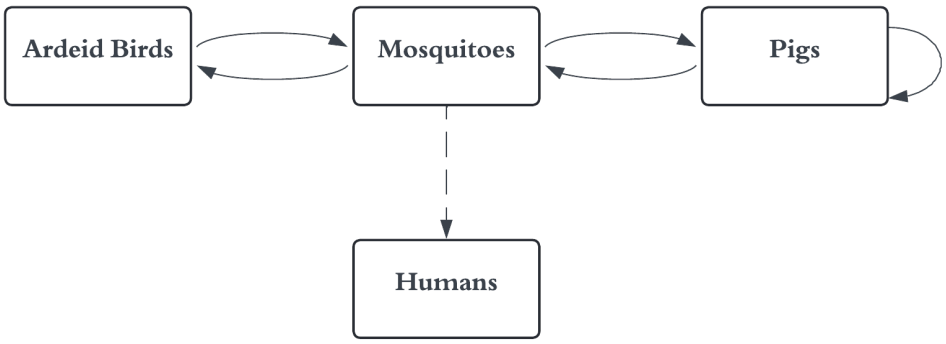

Figure 1: Graphical representation of Japanese encephalitis virus (JEV) transmission cycle. Dashed line indicates transmission to a 'dead-end host'.

endemic countries (Diallo et al. (2018)). One proposed contributor to maintaining endemicity is the presence of feral pigs, since they produce sufficiently high viraemia to infect mosquitoes (Diallo et al. (2018), Lord et al. (2015), Furlong et al. (2023)). Another is that of direct pig-to-pig transmission through oronasal (mouth and nose) secretions (De et al. (2016), Diallo et al. (2018), Ricklin et al. (2016)).

There is much uncertainty about the role of potential pig-to-pig transmission, especially within Australia (Furlong et al. (2022, 2023)). Australia has the world's largest feral pig population, making the role of feral pigs as a reservoir host of specific interest to the Australian context (Furlong et al. (2023)), and the maintained endemicity more likely. High population density of feral pigs means this project is of particular interest for the North Queensland context (Furlong et al. (2023)). Possible endemicity of JEV within northern Australia could have national impact due to the wide distribution of waterbirds (Furlong et al. (2023)) and increased likelihood of incursions into southern Australia, and international impact due to their large range of movements (Furlong et al. (2023)).

2 Statement of Authorship

The research contained within this report is the work of Emma Naumann, under direct supervision of Roslyn Hickson and Justin Sexton. This study is a continuation of Naumann's research undertaken during university coursework, and meets the guidelines of the author's home institution plagiarism policy.

3 Method

3.1 Transmission Model

In this section, we constructed a compartmental model for the dynamics of combined direct pig-to-pig and vector-borne transmission of JEV in feral pig populations (see Fig. 2). For this model, subscripts p and v

were used to indicate pig and vector compartments, respectively. The base model structure corresponding to pig compartments was a susceptible-infectious-recovered model with an additional compartment to capture maternal antibodies for piglets (MSIR). The total population of pigs (N_p) was divided into four compartments, and the female mosquito population (N_v) was divided into two vector compartments. More specifically, the compartments capture the following biology:

1. Pig physiology was considered by including a maternal antibodies compartment ($\hat{M}_p$) to ensure the disease dynamics within pig populations were fully captured. This compartment represents piglets born with maternal antibodies, specifically, piglets born to either infectious, or recovered sows. Piglets transfer to the $\hat{S}_p$ compartment at a rate ψ, which is the waning rate of maternal antibodies.

2. Susceptible pigs ($\hat{S}_p$), are pigs who may become infected after direct contact with an infectious pig. Piglets of susceptible sows are born into this compartment. Whilst biologically inaccurate, to ensure the system balances, piglets born to piglets in the $\hat{M}_p$ compartment are also born into this compartment.

3. Infectious pigs ($\hat{I}_p$), have JEV and may infect susceptible pigs through oronasal secretions. They transition to compartment $\hat{R}_p$ at a rate γ.

4. Recovered pigs ($\hat{R}_p$), are pigs which have recovered from JEV and are no longer infectious. It was assumed that pigs are incapable of re-infection and have lifelong immunity once recovered.

5. Susceptible vectors ($\hat{S}_v$) are vectors that may become infectious after an interaction with an infected pig, and have a force of infection described by $\lambda_{p\to v}$.

6. Infected vectors ($\hat{I}_v$) are vectors that have JEV. They can infect susceptible pigs with a force of infection $\lambda_{v\to p}$.

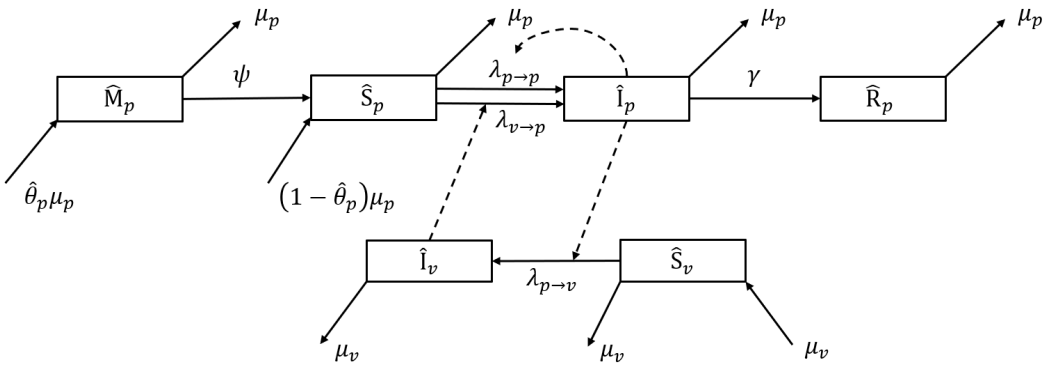

Figure 2: Compartmental model of combined direct and vector-borne JEV transmission.

Only the adult female mosquitoes require blood as a source of nutrients for the development of their eggs,

and hence male mosquitoes are neglected unless modelling intervention methods (see, for example, (Keeling & Rohani (2011))).

Population turnover is a critical component of the long-term behaviour of a transmission model (Keeling & Rohani (2011)). Since the long-term behaviour of the system is of specific interest, demography was included in the model under the assumption of a constant population. Mathematically, this was enforced by equating the birth rate and natural death rate for each species, μ_p and μ_v respectively. Hence, the results are only true for regions with stable feral pig and vector populations. Similarly, 'exposed' compartments were neglected from the model since the period of exposure was short compared to the period of interest.

In Figure 2, the flow into the compartment from births is adjusted by the proportion expected to have maternal antibodies,

$$\hat{\theta} = \frac{\hat{I}_p + \hat{R}_p}{N_p}\,, \tag{1}$$

where $\hat{I}_p$ is the number of infectious pigs, $\hat{R}_p$ is the number of recovered pigs, and N_p is the total feral pig population within a 16 km^2 grid. It was assumed that offspring of sows from $\hat{I}_p$ and $\hat{R}_p$ have perfect inheritance of maternal antibodies, whilst those born into $\hat{S}_p$ do not have any maternal antibodies. Mathematically, $\hat{\theta}_p$ is unitless, leaving the system with the correct overall units given it is multiplied by the birth rate μ_p. Since (1) is unitless and μ_p is a rate, the units are consistent for in-flow and out-flow of each compartment.

The force of infection notation, $\lambda_{x\to y}$ represents the force of infection from species x to species y. Using this notation, the direct transmission force of infection is

$$\lambda_{p\to p} = \beta \hat{I}_p\,, \tag{2}$$

where $\lambda_{p\to p}$ represents the force of infection from direct contact of susceptible and infectious pigs through oronasal secretions, and β is the transmission rate from infectious to susceptible pigs per day (see Table 1). We assumed the direct transmission is density-dependent, where the contact rate and per-capita force of infection increase directly with population density. By letting β equal zero, the direct transmission can be 'switched off', and the contribution of vector-borne transmission can be assessed. From this, it can be determined if vector-borne transmission alone can sustain JEV within a population. The inter-species force of infection terms represent a mosquito biting a pig,

$$\lambda_{v\to p} = \frac{b_{vp} p_{vp} \hat{I}_v}{N_p}\,, \tag{3}$$

$$\lambda_{p\to v} = \frac{b_{vp} p_{pv} \hat{I}_p}{N_p}\,, \tag{4}$$

where b_{vp} describes the vector biting rate, p_{vp} is the probability a susceptible mosquito becomes infected after biting an infectious pig, and p_{pv} is the probability a susceptible pig becomes infected after being bitten by an infectious mosquito (see Table 1). The mosquito compartments can also be 'switched off' by letting the inter-species force of infection terms equal zero.

The dynamics are described by a system of ordinary differential equations (ODEs),

$$\frac{d\hat{M}_p}{dt} = \mu_p(\hat{I}_p + \hat{R}_p) - \mu_p\hat{M}_p - \psi\hat{M}_p\,, \tag{5}$$

$$\frac{d\hat{S}_p}{dt} = \mu_p(\hat{S}_p + \hat{M}_p) + \psi\hat{M}_p - \mu_p\hat{S}_p - \beta\hat{S}_p\hat{I}_p - \frac{b_{vp}p_{vp}\hat{S}_p\hat{I}_v}{N_p}\,, \tag{6}$$

$$\frac{d\hat{I}_p}{dt} = \beta\hat{S}_p\hat{I}_p + \frac{b_{vp}p_{vp}\hat{S}_p\hat{I}_v}{N_p} - \mu_p\hat{I}_p - \gamma\hat{I}_p\,, \tag{7}$$

$$\frac{d\hat{R}_p}{dt} = \gamma\hat{I}_p - \mu_p\hat{R}_p\,, \tag{8}$$

$$\frac{d\hat{S}_v}{dt} = \mu_v N_v - \mu_v\hat{S}_v - \frac{b_{vp}p_{pv}\hat{I}_p\hat{S}_v}{N_p}\,, \tag{9}$$

$$\frac{d\hat{I}_v}{dt} = \frac{b_{vp}p_{pv}\hat{I}_p\hat{S}_v}{N_p} - \mu_v\hat{I}_v\,, \tag{10}$$

$$\hat{M}_p + \hat{S}_p + \hat{I}_p + \hat{R}_p = N_p\,, \tag{11}$$

$$\hat{S}_v + \hat{I}_v = N_v\,. \tag{12}$$

To non-dimensionalise this system such that each compartment represents a proportion of each respective total population N_p and N_v, we let

$$M_p = \frac{\hat{M}_p}{N_p} \tag{13}$$

$$\implies \hat{M}_p = M_p N_p\,. \tag{14}$$

Similarly, all other compartmental variables $(\hat{S}_p, \hat{I}_p, \hat{R}_p, \hat{S}_v, \hat{I}_v)$ were proportionalised. We note the density dependent transmission means N_p is retained in the equations. To determine the effect of this on the behaviour of the model, we then explored how our otherwise-generalised results change for differing values of N_p.

The contact rate (where 'contact' refers to the mosquito biting) and probability of transmission are always multiplied together, and can be combined into a single variable for simplicity. The transmission rates are then

$$T_p = b_{vp}p_{vp}\,, \tag{15}$$

$$T_v = b_{vp}p_{pv}\,, \tag{16}$$

and the ratio of mosquitoes is

$$m = \frac{N_v}{N_p}\,. \tag{17}$$

The system of ODEs becomes

$$\frac{dM_p}{dt} = \mu_p(I_p + R_p) - \mu_p M_p - \psi M_p \,, \tag{18}$$

$$\frac{dS_p}{dt} = \mu_p(S_p + M_p) + \psi M_p - \mu_p S_p - \beta S_p I_p N_p - T_p S_p I_v m \,, \tag{19}$$

$$\frac{dI_p}{dt} = \beta S_p I_p N_p + T_p S_p I_v m - \mu_p I_p - \gamma I_p \,, \tag{20}$$

$$\frac{dR_p}{dt} = \gamma I_p - \mu_p R_p \,, \tag{21}$$

$$\frac{dS_v}{dt} = \mu_v - \mu_v S_v - T_v I_p S_v \,, \tag{22}$$

$$\frac{dI_v}{dt} = T_v I_p S_v - \mu_v I_v \,, \tag{23}$$

$$M_p + S_p + I_p + R_p = 1 \,, \tag{24}$$

$$S_v + I_v = 1 \,. \tag{25}$$

Equations (24) and (25) represent our assumption of a constant total population size for each species, now non-dimensionalised.

3.2 Analytical Analyses

There are multiple analytical analyses we conducted on the model to describe key information about the behaviour of the system.

3.2.1 The Basic Reproduction Number

The basic reproduction number ($\mathcal{R}_0$) is defined as the average number of secondary infections produced by one infectious individual in a fully susceptible population (Diekmann et al. (2010)). $\mathcal{R}_0$ is referred to as a 'threshold value' for deterministic models because for an outbreak to occur, the number of infectious individuals over time must increase, which only occurs if an infectious individual spreads the infection to more than one other individual on average. As such, if $\mathcal{R}_0 > 1$, an outbreak will occur, and if $\mathcal{R}_0 < 1$, an outbreak will not occur. $\mathcal{R}_0$ can be calculated in different ways depending on the complexity of the system of ODEs.

For System (18)–(23) in §3.1, the Next Generation Matrix (NGM) method was used to calculate the basic reproduction number. The NGM relates the number of newly infected individuals within each compartment for consecutive generations (Diekmann et al. (2010)). An infected generation refers to the consecutive infections caused by each infectious individual: the individuals which are infected as a result of an infectious person are referred to as the next generation (Diekmann et al. (2010)). The basic reproduction number is the dominant eigenvalue of the NGM (Diekmann et al. (2010)).

3.2.2 Long-term Behaviour of the System

The steady state, or long-term behaviour, of the system of ODEs describes the infection dynamics when there is no change in the system over time, such as near an endemic steady state solution (Diekmann et al. (2013)).

The two types of steady state solutions we were interested in are the trivial (at disease free equilibrium), and non-trivial steady states. Since we assumed a constant population size, the system is fully described by one less equation per species, and it is not necessary to solve for R_p.

To evaluate the stability of each steady state, the Jacobian (Deisenroth et al. (2020)), and hence eigenvalues, were calculated using symbolic manipulation in MATLAB (2024b). This required use of the 'Symbolic Math Toolbox' MATLAB package for symbolic mathematics (The MathWorks Inc. (2024*b*)). The steady state type was then classified by the characteristics of the Jacobian eigenvalues (positive or negative, real or complex) (Diekmann et al. (2013)).

3.3 Numerical Simulations

An ODE solver was used to solve the system of ODEs. *Ode*45 was used since it is a versatile, high-order ODE solver and has low error: it is the ODE solver of choice when using MATLAB (The MathWorks Inc. (2024*a*)). From this, the transmission dynamics of the system could be observed by parameterising the model using the values provided in Table 1 and plotting the solution.

In the absence of local data to fit the transmission rate, we assumed a critical density of pigs, $N_p = N_{crit}$, was needed for an outbreak to occur in the absence of mosquitoes and calculated the transmission rate (β) from the analytical expression for $\mathcal{R}_0$, by assuming $\mathcal{R}_0 = 1$. We chose $N_{crit} = 5$ ($\beta = 0.0755$) and $N_{crit} = 50$ ($\beta = 0.0077$) to demonstrate an order of magnitude difference in the assumption, within the range of feasible N_p values identified. The values calculated for β are reported in Table 1. A one-way sensitivity analysis was then completed to numerically explore the impact of key parameter values on $\mathcal{R}_0$, and I_p. The parameter ranges detailed in Table 1, specifically the pig population density, ratio of vector to pig population, transmission rate, and pig recovery rate, were varied, and the corresponding $\mathcal{R}_0$ and I_p values calculated.

4 Results

4.1 The Basic Reproduction Number

The basic reproduction number, which was calculated using the NGM method, is

$$\mathcal{R}_0 = \frac{1}{2(\mu_p+\gamma)}\left[\beta N_p + \frac{\sqrt{\mu_v}}{\mu_v}\sqrt{\mu_v(\beta N_p)^2 + 4T_pT_vm(\mu_p+\gamma)}\right]. \tag{26}$$

The full NGM is provided in §A.1.

By 'switching off' inter-species interactions (vector-borne transmission), $\mathcal{R}_0$ for a direct pig-to-pig transmission only model is

$$\mathcal{R}_0 = \frac{1}{2(\mu_p+\gamma)}\left[\beta N_p \pm \sqrt{(\beta N_p)^2}\right] \tag{27}$$

$$= \frac{\beta N_p + \beta N_p}{2(\mu_p+\gamma)} \tag{28}$$

$$= \frac{\beta N_p}{\mu_p+\gamma}. \tag{29}$$

Table 1: Parameter descriptions, expected values and ranges for the transmission model depicted in Figure 2. Rates are per day.

Symbol	Description	Value (Range)	Source(s)
N_p	Pig density in a 16 km^2 grid	5 (1 – 83)	Furlong et al. (2023), West (2008)
m	Ratio of vector to pig population	1 (0 – 100)	Assumed
μ_p	Pig death rate	5.4795 $\times 10^{-4}$	Verbeek (2023)
μ_v	Vector death rate	0.04 (0.033 – 0.047)	Diallo et al. (2018)
ψ	Waning rate of maternal antibodies	0.5055 (0.011 – 1)	Diallo et al. (2018)
β	Transmission rate from infectious to susceptible pigs for $\mathcal{R}_0 = 1$ corresponding to $N_{crit} = 5$ and $N_{crit} = 50$, respectively	0.0755, 0.00766	Calculated based on assumption
N_{crit}	Critical pig population density chosen to calculate β	5, 50	Assumed
b_{vp}	Average vector bite rate	0.25 (0.2 – 0.3)	Diallo et al. (2018)
p_{vp}	Probability a susceptible vector becomes infected after biting an infectious pig	0.56 (0.3 – 0.82)	Diallo et al. (2018)
p_{pv}	Probability a susceptible pig becomes infected after being bitten by an infectious vector	0.205 (0.1 – 0.31)	Diallo et al. (2018)
γ	Pig recovery rate	0.375 (0.25 – 0.5)	Diallo et al. (2018)

Note the inclusion of the N_p term as this is a density dependent transmission model.

Similarly, by 'switching off' the pig-to-pig direct transmission possibility, to capture vector-borne transmission only, $\mathcal{R}_0$ became

$$\mathcal{R}_0 = \frac{1}{2(\mu_p+\gamma)} \frac{\sqrt{\mu_v}}{\mu_v} \sqrt{4T_pT_vm(\mu_p+\gamma)} \tag{30}$$

$$= \frac{\sqrt{4T_pT_vm\mu_v(\mu_p+\gamma)}}{2\mu_v(\mu_p+\gamma)}\,. \tag{31}$$

4.2 Long-term Behaviour of the System

The trivial steady state solution of the combined model is

$$(M_p, S_p, I_p, S_v, I_v) = (0, 1, 0, 1, 0)\,, \tag{32}$$

with the derivation in §A.2.

As shown in §A.3, the non-trivial steady state of the combined model is

$$(M_p, S_p, I_p, S_v, I_v) = \left(\frac{(\mu_p + \gamma) I_p}{\mu_p + \psi}, \frac{(\mu_p + \gamma)(\mu_v + T_v I_p)}{\beta N_p (\mu_v + T_v I_p) + T_p T_v m}, I_p, \frac{\mu_v}{\mu_v + T_v I_p}, \frac{T_v I_p}{\mu_v + T_v I_p} \right), \tag{33}$$

where

$$I_p = \frac{-g_1 \pm \sqrt{g_1^2 - 4 g_2 g_0}}{2 g_2}. \tag{34}$$

This is defined in terms of

$$g_2 = d\beta N_p T_v, \tag{35}$$

$$g_1 = d\beta N_p \mu_v + dc + f T_v - \beta N_p T_v, \text{ and} \tag{36}$$

$$g_0 = f\mu_v - \beta N_p \mu_v - c. \tag{37}$$

In turn, these are defined in terms of

$$d = a + b + 1, \tag{38}$$

$$a = \frac{\mu_p + \gamma}{\mu_p + \psi}, \tag{39}$$

$$b = \frac{\gamma}{\mu_p}, \tag{40}$$

$$c = T_p T_v m, \text{ and} \tag{41}$$

$$f = \mu_p + \gamma. \tag{42}$$

To ensure biological feasibility of the solution, it is required that $I_p > 0$. This condition can be met by ensuring that the following two conditions are satisfied:

$$g_1^2 - 4 g_2 g_0 > 0, \tag{43}$$

$$\text{and, } \sqrt{g_1^2 - 4 g_2 g_0} > g_1. \tag{44}$$

When using values obtained from the literature, the I_p minus case for the non-trivial steady state of the combined model was biologically infeasible since it resulted in negative I_p values. This steady state solution was therefore neglected during the following analyses.

The Jacobian of the combined model was

$$J(M_p, S_p, I_p, S_v, I_v) = \begin{bmatrix} -\mu_p - \psi & 0 & \mu_p & 0 & 0 \\ \mu_p + \psi & -\beta I_p N_p - T_p I_v m & -\beta S_p N_p & 0 & -T_p S_p m \\ 0 & \beta I_p N_p + T_p I_v m & \beta S_p N_p - \mu_p - \gamma & 0 & T_p S_p m \\ 0 & 0 & -T_v S_v & -\mu_v - T_v I_p & 0 \\ 0 & 0 & T_v S_v & T_v I_p & -\mu_v \end{bmatrix}. \tag{45}$$

The eigenvalues corresponding to both the trivial and non-trivial state were evaluated using symbolic mathematics in MATLAB and found to be analytically intractable.

4.3 Numerical Simulations

Figure 3 depicts the transmission dynamics of the proposed model during a 10 year period, for parameter values from Table 1, and values of $\mathcal{R}_0$ corresponding to both $\beta = 0.0755$ (Fig. 3a), and $\beta = 0.0077$ (Fig. 3b) solved using *ode*45. A ten year study period was chosen to ensure that the long-term behaviour was reached for each solution. The initial proportion of S_p and S_v were 0.99 of each respective population. From Figure 3a, it is evident that the system tends towards the steady state solution after approximately 550 days, with peak pig infection of 0.79 on day 2 of the outbreak. The peak vector incidence occurs on day 8, with 0.11 of the population being infected. The solution corresponding to $\beta = 0.0077$, exhibits a series of outbreaks, and the steady state solution is not reached within the 10 year simulation. The peak pig infection proportion is 0.17 after 12 days of disease outbreak, and the peak vector incidence occurs on day 20 with 0.07 of the population infected (Fig. 3b).

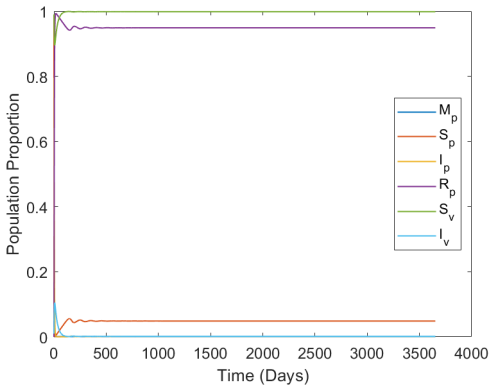

(a) Model solution for $\beta = 0.0755$ ($N_{crit} = 5$).

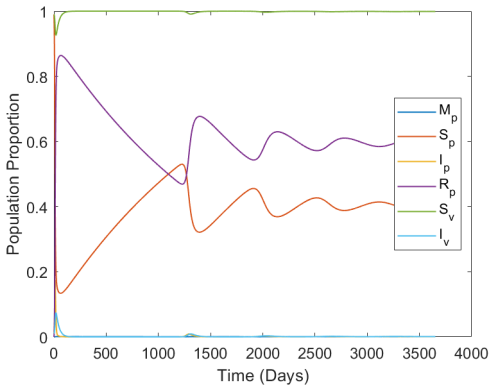

(b) Model solution for $\beta = 0.0076$ ($N_{crit} = 50$).

Figure 3: Numeric solutions for differing β values, $N_p = 100$, $m = 1$, and the remaining parameter values per Table 1.

The cumulative pig and vector incidence is depicted in Figure 4. The cumulative pig and vector incidence corresponding to $\beta = 0.0755$ has a sharp increase in the first 2 days of the simulation, then plateaus until approximately day 200 of the outbreak, before exhibiting a linearly increasing relationship throughout the remainder of the 10 year simulation (Fig. 4a). This corresponds to a constant increase due to having reached an endemic steady state. The maximum cumulative incidence for this case is 2.84 for pigs, and 0.38 for vectors. Figure 4b, which is the cumulative incidence for the $\beta = 0.0077$ case, has a sharp increase for the first approximately 50 days, before plateauing, and then exhibiting a series of rapid increases in cumulative incidence for the remainder of the ten year period. The maximum cumulative incidence is 1.81 and 0.2428, for pigs and vectors respectively. For both cases, the cumulative incidence of pigs is approximately triple that of the vectors.

By letting $\beta = 0$, the direct transmission was turned off (vector-borne only), and the effect on the system dynamics is depicted in Figure 5a. Figure 5a depicts a peak pig infection proportion of 0.01 and a peak vector infection proportion of 0.01. Peak infection occurs after 1 day of an outbreak for the pig population, and 2 days

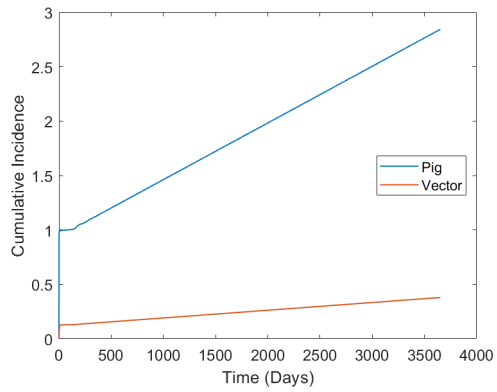

(a) Cumulative incidence for $\beta = 0.0755$ ($N_{crit} = 5$).

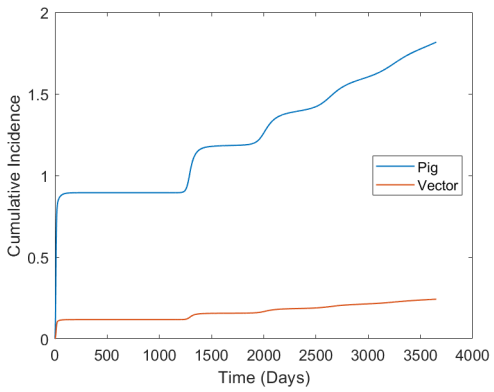

(b) Cumulative incidence for $\beta = 0.0076$, ($N_{crit} = 50$).

Figure 4: Cumulative pig incidence over time (days) for differing β values, $N_p = 100$, $m = 1$, and the remaining parameter values per Table 1.

for the vector population. The cumulative pig and vector incidence for the $\beta = 0$ case is depicted in Figure 5b. This figure exhibits a large, rapid increase in cumulative incidence for both species, during approximately the first 250 days for pigs, and 150 days for vectors. The maximum cumulative pig incidence for this case is 0.07, and the maximum cumulative vector incidence is 0.01.

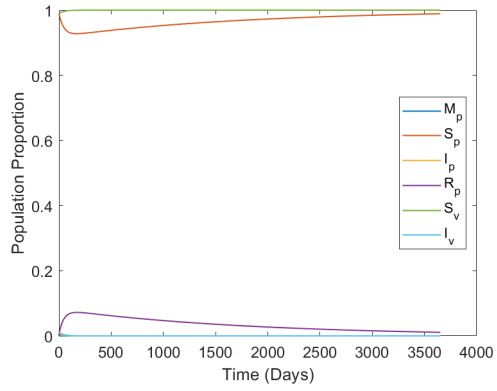

(a) Model solution.

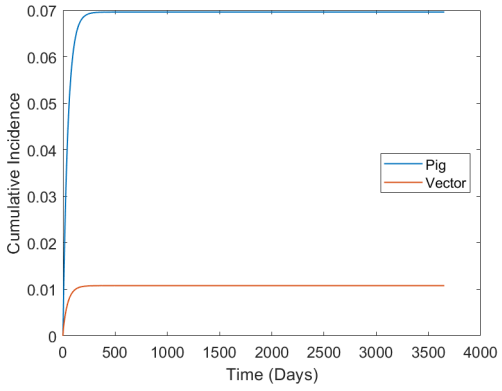

(b) Cumulative incidence.

Figure 5: Model solution and cumulative incidence over time (days) for $\beta = 0$, $N_p = 100$, $m = 1$, and the remaining parameter values per Table 1.

4.4 Sensitivity Analysis of the Basic Reproduction Number with Population Density

Figure 6a depicts how the basic reproduction number changes with pig population N_p, for three different transmission rate cases. We explored the maximum estimated pig density of 1 to 83 pigs in a 16 km^2 grid

(Table 1). All three transmission rate cases have $\mathcal{R}_0$ values greater than 1, for the entire range of pig population densities reported. The most interesting result here is the non-monotonic relationship between $\mathcal{R}_0$ and N_p for $\beta = 0.07555$, suggesting further exploration of the dynamics could yield interesting results. The maximum $\mathcal{R}_0$ value is 21.96, corresponding to $\beta = 0.0755$ and $N_p = 1$. For high feral pig population densities, specifically $N_p = 83$, the $\mathcal{R}_0$ value corresponding to $\beta = 0.0755$ is 17.02, compared to the $\beta = 0.0077$ and $\beta = 0$ cases which have $\mathcal{R}_0$ values of 3.39 and 2.40, respectively.

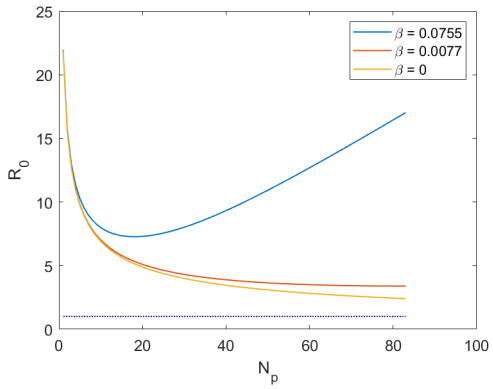

(a) $\mathcal{R}_0$ as a function of pig population density, for three transmission rate cases, where $m = 1$. N_p is varied from 1 to 83 as an informed estimate of pig density in a 16 km^2 grid, as per Table 1.

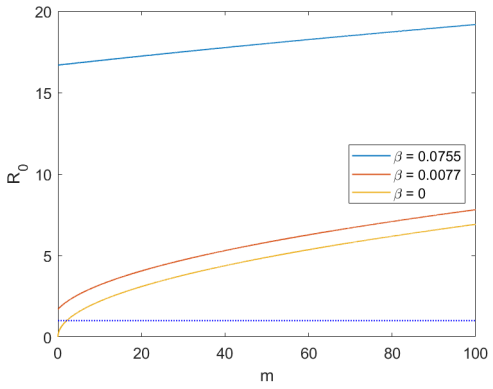

(b) $\mathcal{R}_0$ as a function of vector to pig population ratio (m) for three transmission rate cases, where $N_p = 83$.

Figure 6: One-way sensitivity analysis, varying N_p and m, to determine the effect on $\mathcal{R}_0$. The dotted lines corresponds to $\mathcal{R}_0 = 1$.

The relationship between the basic reproduction number and m is demonstrated in Figure 6b for three transmission rates. This figure explores the effect of vector-borne transmission on the basic reproduction number. The dotted line represents $\mathcal{R}_0 = 1$. All three transmission rates exhibit an increasing relationship between m and $\mathcal{R}_0$. The $\beta = 0.0077$ and $\beta = 0$ cases have the greatest increase in $\mathcal{R}_0$ values occurring approximately when $0 < m < 20$. The case corresponding to $\beta = 0.0755$, results in $\mathcal{R}_0$ values approximately 2.5 to 9 times greater than the $\beta = 0.0077$ case, for every value of m. The $\mathcal{R}_0$ values corresponding to $\beta = 0.0077$ are consistently 1 to 1.5 times greater than the $\beta = 0$ case. The case without direct pig-to-pig transmission ($\beta = 0$), has $\mathcal{R}_0$ values < 1 for values of $m < 2.11$. In contrast, the $\beta = 0.0755$ and $\beta = 0.0077$ cases have values of $\mathcal{R}_0 > 1$ for all values of m.

4.5 Sensitivity Analysis of $\mathcal{R}_0$ and I_p to Assumed Parameter Values

Figure 7a depicts an approximately linearly increasing relationship between β and $\mathcal{R}_0$. Whereas, in Figure 7b, increasing γ results in a decrease in $\mathcal{R}_0$ for all beta values. The largest beta value ($\beta = 0.0755$) corresponds to $\mathcal{R}_0$ values approximately 8 times those of $\beta = 0.0077$ (Fig. 7b). I_p is most sensitive to changes in small

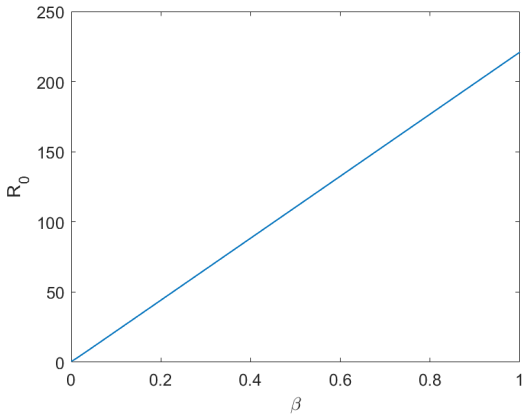

(a) Sensitivity of $\mathcal{R}_0$ to changes in β

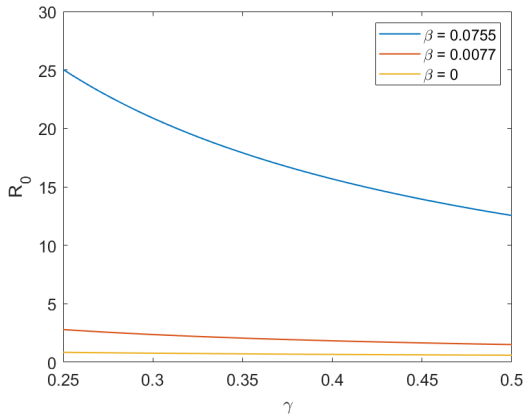

(b) Sensitivity of $\mathcal{R}_0$ to changes in γ

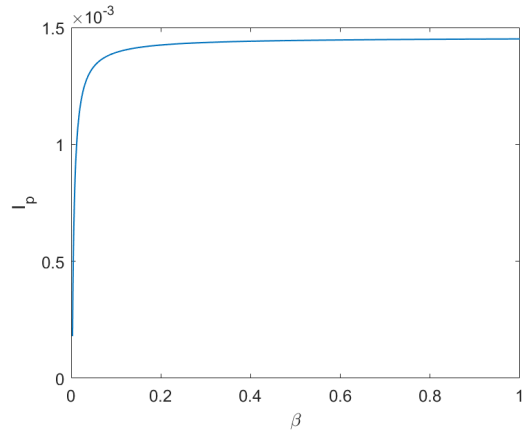

(c) Sensitivity of I_p to changes in β

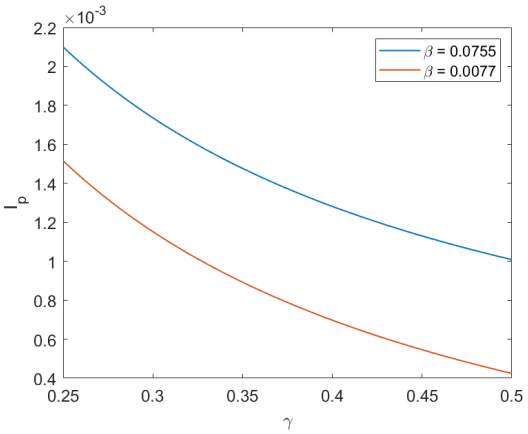

(d) Sensitivity of I_p to changes in γ

Figure 7: One-way sensitivity analysis, varying β and γ, to determine the effect on $\mathcal{R}_0$ (a,b) and I_p (c,d).

values of β, specifically $0.003 < \beta < 0.35$ (Fig. 7c). Values of $\beta < 0.003$ were not plotted since they resulted in biologically infeasible values of I_p ($I_p < 0$). In Figure 7d, the $\beta = 0$ case was not plotted since it resulted in undefined values of I_p for every γ value. Similarly to Figure 7b, as γ increases, I_p decreases. Values of I_p corresponding to $\beta = 0.0755$ are approximately 1.4 to 2 times greater than values of I_p corresponding to $\beta = 0.0077$.

5 Discussion

From Figure 3a it is evident that for small N_{crit} and hence large β, an initial large outbreak occurs, resulting in more than 90% of the pig population becoming infected and then recovered. Following this, a series of small outbreaks occurs before the system tends towards an endemic steady state solution. Since the initial outbreak caused such a large proportion of the pig population to transition to the R_p compartment, and the model assumed life-long immunity for recovered pigs, the S_p compartment remained too small for large outbreaks to

occur. This dynamic is reflected in Figure 4a, where a rapid increase in cumulative incidence of both vectors and pigs is followed by the system tending towards a linearly increasing cumulative incidence. Figure 3b depicts the transmission dynamics when the model was parameterised using a larger N_{crit}, and hence a smaller β. The smaller direct transmission rate has resulted in a smaller initial outbreak. Since less of the pig population has life-long immunity, the system experiences a series of much larger outbreaks than in Figure 3a. This model does not reach the endemic steady state within the ten year simulation, however, it is tending towards a more endemic steady state than the model corresponding to a larger β. Fig. 3b corresponds to this model solution, showing the cumulative incidence and exhibiting the same dynamics: a large initial increase followed by a series of spikes which represent outbreaks. Therefore, a larger β value results in a larger initial outbreak, and a shorter time to reach the endemic steady state (Fig. 3). Since β was calculated such that $\mathcal{R}_0 > 1$ and hence an outbreak would occur, these model solutions reflect the expected system dynamics.

Figure 5a is the model solution for $\beta = 0$. Whilst an initial outbreak can be observed, the system tends towards the trivial steady state solution described by Equation 32 for the remaining duration of the simulation. This relationship is also depicted in Figure 5b, where the cumulative incidence plateaus after an initial increase. From this model solution, it can be determined that when parameterised with the values contained in Table 1, the system does not tend towards an endemic steady state without the contribution of direct pig-to-pig transmission. It should also be noted that the proposed transmission model is a conservative estimate of when JEV could become endemic since it neglects the contribution of Ardeid birds to this dynamic process. Further research would be necessary to determine β for the Australian context, and hence whether the Australian steady state solution would be endemic. However, this modelling does suggest feral pigs could be a significant contributor to achieving endemicity in Australia.

By decreasing the transmission rate by an order of magnitude, from $\beta = 0.0755$ to $\beta = 0.0076$, corresponding to $N_{crit} = 5$ and $N_{crit} = 50$ respectively, a decrease of 0.62 can be observed for peak pig incidence, and 0.04 for peak vector incidence (Fig. 3). In addition to a decrease in maximum incidence for both populations, the peak occurred 10 days later for pigs, and 12 days later for vectors. This is further evident for the $\beta = 0$ model: the peak infection proportion has a decrease of 0.16 for pigs, and 0.06 for vectors, when compared to the $\beta = 0.0077$ case. Whilst the increase in time required to reach maximum pig incidence is only on the scale of days, rather than years, and is not significant when considering long-term steady state dynamics, this may be significant if intervention strategies are included in the model. Future models could potentially include intervention strategies such as vaccination and mosquito control strategies to determine the effect on transmission dynamics. Dissimilarly, the peak for pigs occurs 11 days earlier, and 18 days earlier for peak vector incidence. Hence, with the removal of direct pig-to-pig transmission, the peak incidence of both populations is reduced, and the timeline of the initial outbreak is shortened.

The cumulative incidence for both pigs and vectors decreases with a decreasing pig transmission rate (Fig. 4 and Fig. 5b). There is a decrease of 2.77 for pigs, and 0.37 for vectors, when comparing the $\beta = 0.0755$ and $\beta = 0$ solutions. Hence, by reducing the direct oronasal transmission rates, the cumulative number of infected pigs has a 97.5% decrease after turning off direct transmission. Turning off direct transmission also

decreases the maximum cumulative vector incidence by 97.4%. As such, the direct pig-to-pig transmission of JEV could contribute heavily to the endemicity of JEV within Australia, especially during months when mosquito populations decline, as evidenced by the increase in peak and cumulative incidence when considering larger β values.

Future models may need to consider differences in the dynamics between feral and domestic pigs to determine the effect on the disease dynamics and hence the generality of this model. Differences in dynamics could include differing lifespans, as well as contact rates with other pigs and mosquitoes due to biosecurity measures within domestic piggeries (Australian Pork Limited (2022)). Since there are almost no domestic piggeries in North Queensland the contribution of domestic pigs to the JEV transmission cycle can be considered negligible and was hence excluded, however, this may not be possible in regions with more domestic piggeries.

Whilst all three transmission rates in Figure 6a have $\mathcal{R}_0$ values greater than 1 for all N_p values, only the $\beta = 0.0755$ case has an increasing relationship between values of $N_p > 20$ and $\mathcal{R}_0$. In particular the non-monotonicity of the relationship between $\mathcal{R}_0$ and N_p could result in complicated and potentially perverse outcomes from feral pig population controls, though this would require substantial further investigation. The other two cases both exhibit a decreasing relationship between N_p and $\mathcal{R}_0$ for all values of N_p. The largest difference in $\mathcal{R}_0$ values across the three cases occurs for $N_p = 83$, the maximum feral pig population density in a 16 km^2 area (Fig. 6a). For $N_p = 83$, $\mathcal{R}_0$ decreases by 14.62 when comparing the $\beta = 0.0755$ and $\beta = 0$ cases. Hence, from Figure 6a it is evident that the contribution of direct pig-to-pig transmission to secondary infections is negligible for small values of N_p, and much greater for higher values of N_p.

As expected of this model, $\mathcal{R}_0$ increases with m (Fig. 6b). Direct transmission has a significant effect on $\mathcal{R}_0$ when varying m, for a high direct transmission rate ($\beta = 0.0755$). For low direct transmission rates ($\beta = 0.0077$ and $\beta = 0$), the ratio of vector to pig population has a significant effect on the value of $\mathcal{R}_0$, especially when $0 < m < 20$. For the $\beta = 0.0755$ and $\beta = 0.0077$ cases, $\mathcal{R}_0$ is greater than 1 for every m value, including $m = 0$, meaning that direct transmission alone can sustain an outbreak. For $\beta = 0$, $\mathcal{R}_0$ was < 1 for $m < 2.11$, meaning that vector-borne transmission is required for an outbreak to occur for low values of m. Hence, the contribution of direct transmission is significant when m is small, and could have a wide-reaching impact on both agriculture and human health by increasing peak infection proportion and hence cumulative incidence, decreasing the time to peak outbreak, and increasing the number of secondary infections per individual in each generation. Further sensitivity analyses with respect to key model parameters (Fig. 7) show how the threshold condition and endemicity ($I_p > 0$) are affected by changes, emphasising the need for further studies.

In addition to high feral pig densities surrounding Townsville, three different mosquito types which have been identified as possible vectors of JEV exist in the region (Furlong et al. (2023)), further contributing to the possibility of JEV endemicity in the region. The parameter spaces with feasible endemic equilibria highlights the need for local studies to better understand the local disease ecology, as our parameters were based on assumptions and are taken from a range of Southeast Asian contexts.

References

Australian Pork Limited (2022), 'Australian Pork Industry Quality Assurance Program (APIQ) Standards Manual'.

De, A., Maity, K., Jana, S. & Maiti, M. (2016), 'Application of various control strategies to Japanese encephalitic: A mathematical study with human, pig and mosquito', *Mathematical Biosciences* **282**, 46–60.

Deisenroth, M. P., Faisal, A. A. & Ong, C. S. (2020), *Mathematics for machine learning*, Cambridge University Press, Cambridge ; New York, NY.

Diallo, A. O. I., Chevalier, V., Cappelle, J., Duong, V., Fontenille, D. & Duboz, R. (2018), 'How much does direct transmission between pigs contribute to Japanese Encephalitis virus circulation? A modelling approach in Cambodia', *PLOS ONE* **13**(8), e0201209.

Diekmann, O., Heesterbeek, H. & Britton, T. (2013), *Mathematical tools for understanding infectious diseases dynamics*, Princeton series in theoretical and computational biology, Princeton University Press, Princeton.

Diekmann, O., Heesterbeek, J. A. P. & Roberts, M. G. (2010), 'The construction of next-generation matrices for compartmental epidemic models', *Journal of The Royal Society Interface* **7**(47), 873–885.

Furlong, M., Adamu, A., Hickson, R., Horwood, P., Golchin, M., Hoskins, A. & Russell, T. (2022), 'Estimating the Distribution of Japanese Encephalitis Vectors in Australia Using Ecological Niche Modelling', *Tropical Medicine and Infectious Disease* **7**(12), 393.

Furlong, M., Adamu, A. M., Hoskins, A., Russell, T. L., Gummow, B., Golchin, M., Hickson, R. I. & Horwood, P. F. (2023), 'Japanese Encephalitis Enzootic and Epidemic Risks across Australia', *Viruses* **15**(2), 450.

Goondiwindi Regional Council (2025), Queensland Japanese Encephalitis Virus Update 2-17 January 2025, Technical report, Goondiwindi Regional Council.
URL: *https://grc.qld.gov.au/News-and-Events/News/Council-News/2025/Queensland-Japanese-Encephalitis-Virus-Update-2-%E2%80%93-17-January-2025*

Keeling, M. J. & Rohani, P. (2011), *Modeling Infectious Diseases in Humans and Animals*, Princeton University Press.

Khan, S. U., Salje, H., Hannan, A., Islam, M. A., Bhuyan, A. A. M., Islam, M. A., Rahman, M. Z., Nahar, N., Hossain, M. J., Luby, S. P. & Gurley, E. S. (2014), 'Dynamics of Japanese Encephalitis Virus Transmission among Pigs in Northwest Bangladesh and the Potential Impact of Pig Vaccination', *PLoS Neglected Tropical Diseases* **8**(9), e3166.

Klein, M. J., Jackson, S. A., Suen, W. W., Payne, J., Beveridge, D., Hargreaves, M., Gillies, D., Wang, J., Blasdell, K. R., Dunn, M., López-Denman, A. J., Durr, P. A., Williams, D. T. & Paradkar, P. N. (2024),

'Australian Culex annulirostris mosquitoes are competent vectors for Japanese encephalitis virus genotype IV', *Emerg Microbes Infect* **13**(1), 2429628.

Lord, J. S., Gurley, E. S. & Pulliam, J. R. C. (2015), 'Rethinking Japanese Encephalitis Virus Transmission: A Framework for Implicating Host and Vector Species', *PLOS Neglected Tropical Diseases* **9**(12), e0004074.

McGrath, Christian (2025), Japanese encephalitis in Victoria this summer, Technical report, Health.vic. **URL:** *https://www.health.vic.gov.au/health-alerts/japanese-encephalitis-in-victoria-this-summer*

Mulvey, P., Duong, V., Boyer, S., Burgess, G., Williams, D. T., Dussart, P. & Horwood, P. F. (2021), 'The Ecology and Evolution of Japanese Encephalitis Virus', *Pathogens* **10**(12), 1534.

Ricklin, M. E., García-Nicolás, O., Brechbühl, D., Python, S., Zumkehr, B., Nougairede, A., Charrel, R. N., Posthaus, H., Oevermann, A. & Summerfield, A. (2016), 'Vector-free transmission and persistence of Japanese encephalitis virus in pigs', *Nature Communications* **7**(1), 10832.

The MathWorks Inc. (2024*a*), 'Matlab version: 24.2.0.2712019 (r2024b)'.

The MathWorks Inc. (2024*b*), 'Symbolic math toolbox version: 24.2 (r2024b)'.

Verbeek, B. (2023), 'Biology, ecology and impacts'.

Wadman, M. (2023), 'Rude awakening', *Science* **382**(6673), 872–877.

West, P. (2008), *Assessing invasive animals in Australia*, National Land & Water Resources Audit, Bradon, ACT. OCLC: 277184107.

A Appendix: Derivations of key epidemiological metrics

A.1 $\mathcal{R}_0$ calculation using the NGM method

The NGM is

$$K_L = \begin{bmatrix} \frac{\beta N_p}{\mu_p+\gamma} & \frac{T_p m}{\mu_v} \\ \frac{T_v}{\mu_p+\gamma} & 0 \end{bmatrix}. \tag{46}$$

Since $\mathcal{R}_0$ is the dominant eigenvalue,

$$\lambda = \frac{1}{2(\mu_p+\gamma)}\left[\beta N_p + \frac{\sqrt{\mu_v}}{\mu_v}\sqrt{\mu_v(\beta N_p)^2 + 4T_pT_vm(\mu_p+\gamma)}\right]. \tag{47}$$

A.2 Trivial Steady State Solution

In the standard way, for steady state solution there is no change with respect to time, hence the left hand side of the system of ODEs equals zero. Then, from (21),

$$R_p = \frac{\gamma}{\mu_p} I_p \,. \tag{48}$$

Substitute Eqn (48) into Eqn (18), and rearrange to find

$$M_p = \frac{(\mu_p + \gamma)}{\mu_p + \psi} I_p \,. \tag{49}$$

From Equation (22),

$$S_v = \frac{\mu_v}{\mu_v + T_v I_p} \,. \tag{50}$$

Substitute Eqn (50) into Eqn (23),

$$I_v = \frac{T_v I_p}{\mu_v + T_v I_p} \,. \tag{51}$$

Substitute (51) into (20),

$$I_p \left(\beta S_p N_p + \frac{T_p T_v S_p m}{\mu_v + T_v I_p} - \mu_p - \gamma \right) = 0 \,, \tag{52}$$

$$\therefore I_p = 0 \text{ or, } S_p \left(\beta N_p + \frac{T_p T_v m}{\mu_v + T_v} \right) = \mu_p + \gamma \,. \tag{53}$$

Therefore, the trivial steady state can be found by substituting Eqn (53) into Equations (48) and (49), and then all of these equations into Eqn (24). Therefore,

$$S_p = 1 \,. \tag{54}$$

Also, substituting Eqn (53) into Eqn (25), results in:

$$S_v + I_v = 1 \,, \tag{55}$$

$$\therefore S_v = 1 \,. \tag{56}$$

Hence, the trivial steady state for the combined transmission model is,

$$(M_p, S_p, I_p, S_v, I_v) = (0, 1, 0, 1, 0) \,. \tag{57}$$

A.3 Non-Trivial Steady State Solution

The non-trivial steady state can be determined using Equation (53), by first rearranging the equation,

$$S_p = \frac{(\mu_p + \gamma)(\mu_v + T_v I_p)}{\beta N_p (\mu_v + T_v I_p) + T_p T_v m} \,. \tag{58}$$

Then, substituting Equations (48), (49), and (58) into Equation (24),

$$\frac{(\mu_p + \gamma)}{\mu_p + \psi} I_p + \frac{\gamma}{\mu_p} I_p + I_p + \frac{(\mu_p + \gamma)(\mu_v + T_v I_p)}{\beta N_p (\mu_v + T_v I_p) + T_p T_v m} = 1 \,. \tag{59}$$

For simplicity, let,

$$a = \frac{\mu_p + \gamma}{\mu_p + \psi}\,, \tag{60}$$

$$b = \frac{\gamma}{\mu_p}\,, \tag{61}$$

$$c = T_p T_v m\,, \tag{62}$$

$$f = \mu_p + \gamma\,. \tag{63}$$

Letting $d = a + b + 1$,

$$I_p^2(d\beta N_p T_v) + I_p(d\beta N_p \mu_v + dc + fT_v - \beta N_p T_v) + f\mu_v - \beta N_p \mu_v - c = 0\,. \tag{64}$$

For simplicity, let

$$g_2 = d\beta N_p T_v\,, \tag{65}$$

$$g_1 = d\beta N_p \mu_v + dc + fT_v - \beta N_p T_v\,, \tag{66}$$

$$g_0 = f\mu_v - \beta N_p \mu_v - c\,. \tag{67}$$

Using the quadratic formula,

$$I_p = \frac{-g_1 \pm \sqrt{g_1^2 - 4g_2 g_0}}{2g_2}\,. \tag{68}$$